ELSEVIER

Physica C 303 (1998) 191–201

PHYSICA C

Comparative study of global and local magnetization measurements on single crystalline high-T_c superconductors

M. Werner [a], G. Brandstätter [a], F.M. Sauerzopf [a], H.W. Weber [a,*], A. Hoekstra [b], R. Surdeanu [b], R.J. Wijngaarden [b], R. Griessen [b], Y. Abulafia [c], Y. Yeshurun [c], K. Winzer [d], B.W. Veal [e]

[a] *Atominstitut der Österreichischen Universitäten, 1020 Vienna, Austria*
[b] *Institute COMPAS and Faculty of Physics and Astronomy, Vrije Universiteit, 1081 HV Amsterdam, The Netherlands*
[c] *Department of Physics, Bar Ilan University, Ramat Gan, Israel*
[d] *Physikalisches Institut, Universität Göttingen, 37073 Göttingen, Germany*
[e] *Materials Science Division, Argonne National Laboratory, Argonne, IL 60439, USA*

Received 15 March 1998; revised 13 May 1998; accepted 20 May 1998

Abstract

The mixed state of several (RE)$Ba_2Cu_3O_{7-\delta}$ single crystals (RE = Y,Yb) was investigated by various measuring techniques. Using an 8 T SQUID magnetometer as a reference, we compare the current densities evaluated from global magnetization measurements (SQUID, torque and VSM) and from a local technique (Hall probe array). Taking the specific time scales of the various measurements into consideration, we obtain excellent agreement at all temperatures from 5 to 77 K. Magneto-optical images of the flux density gradients confirm that the current densities can be calculated on the basis of an extended Bean model. The established correspondence between global and local techniques is of fundamental relevance for future experimental work on the subject.

Keywords: SQUID; Torque magnetometer; Hall probe array

1. Introduction

Because magnetization measurements on single crystalline high temperature superconductors (HTS) are based on many different experimental techniques, a comparison between them is of significant importance.

Firstly, we address so-called 'global' magnetization methods such as SQUID, torque and vibrating sample magnetometry (VSM). What these techniques have in common is that they are based on the detection of the magnetic moment m integrated over the entire sample, but they employ different methods to detect the magnetic response. The evaluation of the current density J_c from these experiments is based on the critical state equation:

$$\boldsymbol{P}_L = \boldsymbol{J}_c \times \boldsymbol{B} = \mathrm{rot}\,\boldsymbol{H} \times \boldsymbol{B} = (\mathrm{rot}\,\boldsymbol{B} \times \boldsymbol{B}) \frac{\partial H}{\partial B} = -\boldsymbol{P}_v \quad (1)$$

* Corresponding author. Tel.: +43-1-72701-240; Fax: +43-1-7289220; E-mail: weber@ati.ac.at

0921-4534/98/$19.00
PII S0921-4534(98)00259-7

where J_c is the critical current density, $\mu_0 H$ is the applied field, B is the magnetic induction, P_L is the driving Lorentz force and P_v is the pinning force. Hence, J_c can be assessed from the corresponding flux density gradient built up by the pinning centers. As the gradient is not observable directly by these techniques, the usual way is to convert the measured magnetic moment m into the magnetization $M = m/V$, where V is the sample volume and M is a function of the external field. Then, the current density is calculated from the Bean model [1,2] and/or its extensions for finite geometry and demagnetization effects. Relaxation, which affects the flux line lattice (FLL), leads to a time dependence of the current density. In the following, we will always refer to $J(t > 0)$, thus, the measured $J = J_s$ is always less than the 'true' critical current density. [1] As a consequence of the time dependence of J, when comparing different experimental methods, we have to take their different time scales into account. SQUID measurements are characterized by a high accuracy (especially at low fields), but involve long time scales due to the necessary field stabilization. The advantage of torque magnetometry lies in its high accuracy at higher fields and its quick response time, which allows to investigate the dynamics of the flux line lattice as well as magnetic field loops at different sweep rates. Similar to the torque magnetometer the VSM allows to choose different sweep rates and to investigate the dynamics of the FLL due to its quick response time. However, the disadvantage is the lower accuracy especially at high temperatures and high fields compared to a SQUID.

Beside these global methods, techniques such as microscopic Hall probes or magneto-optics (MO) have been developed in order to investigate the local field distribution. Taking advantage of well known effects, both techniques detect the variation of the 'local' magnetic induction B profile within the sample. Although the current density J_s can be determined from both types of experiments [3,4] (with certain assumptions), we used in the present study the MO images only for assessing the sample quality, and calculated the current density from local Hall probe measurements.

This paper will first concentrate on experimental details as discussed in Section 2, where we describe the crystals and aspects of the evaluation process related to each technique, then we present comparisons between the various techniques in Section 3, and draw conclusions in Section 4.

2. Experimental details

2.1. Samples

Three (RE)$Ba_2Cu_3O_{7-\delta}$ single crystals were investigated. Some of their physical properties are summarized in Table 1. The crystallographic quality of all samples was studied by X-ray diffraction and found to be excellent. Furthermore, the magneto-optical (MO) images taken of the samples proved their good quality, i.e., the absence of major defects, through the uniform flux penetration patterns. Crystal M3944 has an oxygen content of around 6.8 and M3976 of 6.76 and their critical temperatures are 83.1 K and 79.3 K, respectively. Table 2 summarizes the different experimental techniques employed for each crystal. All measurements were done in magnetic fields applied parallel to the crystallographic c-axis.

2.2. SQUID magnetometry

The great advantage of resolving very small magnetic moments ($\leq 10^{-10}$ A m^2) made Superconducting Quantum Interference Devices (SQUIDs) [5] the most common equipment for global magnetization measurements on small bulk samples.

SQUID measurements in fields up to 8 T were carried out in a non commercial VTS-800-SQUID magnetometer (referred to as the HF-SQUID) designed by SHE-corporation [6]. It consists of an 8 T magnet surrounding the sample chamber and the transverse and axial SQUID sensors. The latter was used throughout the experiments. The pick-up coil system is designed as a first order gradiometer and

[1] In the following, J is called the shielding current density (J_s), in order to make the difference between $J_c \equiv J(t = 0)$ and $J(t > 0)$ more obvious.

Table 1
Sample properties

Sample code	Type	From	Dimension (mm^3)	Mass (mg)	T_c (K)
M3944	Y-123	Argonne	$1.06 \times 0.644 \times 0.313$	1.398(9)	83.1
M3976	Y-123	Argonne	$1.513 \times 0.988 \times 0.244$	2.395(3)	79.3
Göttl	Yb-123	Göttingen	$1.576 \times 0.608 \times 0.0381$	0.265(4)	89.11

provides a resolution of 10^{-10} A m^2. The temperature is measured with a resolution of 0.01 K. We use a special aluminum sample holder [7], which enables a very accurate orientation of the sample with respect to the field direction. In order to allow reproducibility of the crystal mounting, all samples are glued onto an U-shaped aluminum foil, which fits exactly into a slot in the sample holder. During each measurement cycle, the sample moves four times through the upper and the lower pick-up coil, while the signal is recorded three times per second, thus giving roughly 1500 data points per file. The measured signal is a superposition of the individual signals of the sample and of the sample holder. To determine the signal of the sample holder, a measurement above the transition temperature is made. Disregarding the small temperature dependence of this signal, it is subtracted from the data measured below T_c. From the remaining signal, the magnetic moment is calculated.

The analysis of the data is based on an extended Bean model [8], which evaluates the current density J_s in terms of Bean's critical state model, [2] taking the generated local self field H_{self}, the influence of the anisotropy of the samples at different field orientations and the demagnetization factor into account.

2.3. Torque magnetometry

The torque measurements were performed with a capacitance torque magnetometer. The setup is based on the principles originally developed by Griessen [9,10], to investigate the de Haas–van Alphen effect. Despite its simplicity, the method has some advantages compared to a SQUID. The main advantage is that it is the only apparatus which measures directly the magnetic moment $\propto$ current $\times$ area. Furthermore, it does not suffer from demagnetization factor-effects: it is thus ideally suited for thin films and/or anisotropic bulk samples since $\boldsymbol{m} \| \boldsymbol{c}$.

The torque $\boldsymbol{\tau}$ exerted on a superconducting sample with a magnetic moment $\boldsymbol{m}$ in an external magnetic field $\boldsymbol{B}_e = \mu_0 \boldsymbol{H}_e$ is given by

$$\boldsymbol{\tau} = \boldsymbol{m} \times \boldsymbol{B}_e = m \cdot B_e \cdot \sin\alpha, \quad (2)$$

where α is the angle between the magnetic moment and the external field. Eq. (2) shows that the torque vanishes, when the magnetic moment is parallel to the applied field.

The torquemeter consists of two (0.1 mm thick) identical springs made of phosphorus–bronze foil and is mounted at a fixed angle $\alpha = 5 \pm 0.05°$ between the magnetic field and the c-axis. The sample and the calibration coil are glued on top of the upper spring. The maximum sweep rate of the 7 T magnet is 40 mT/s. A temperature stabilization to better than 0.1 K is realized by simultaneously regulating the helium flow through the heat exchanger and a heater via a PID control system.

The external magnetic field induces a magnetic moment in the sample and exerts a torque on it. The sample slightly tilts until the mechanical torque of the spring balances the magnetic torque. Thus, there

Table 2
Measurements methods

Sample code	SQUID	Torque	VSM	Hall probes	MO
M3944	x	–	–	x	x
M3976	x	–	x	–	x
Göttl	x	x	–	–	x

[2] This approach is valid only above full field penetration.

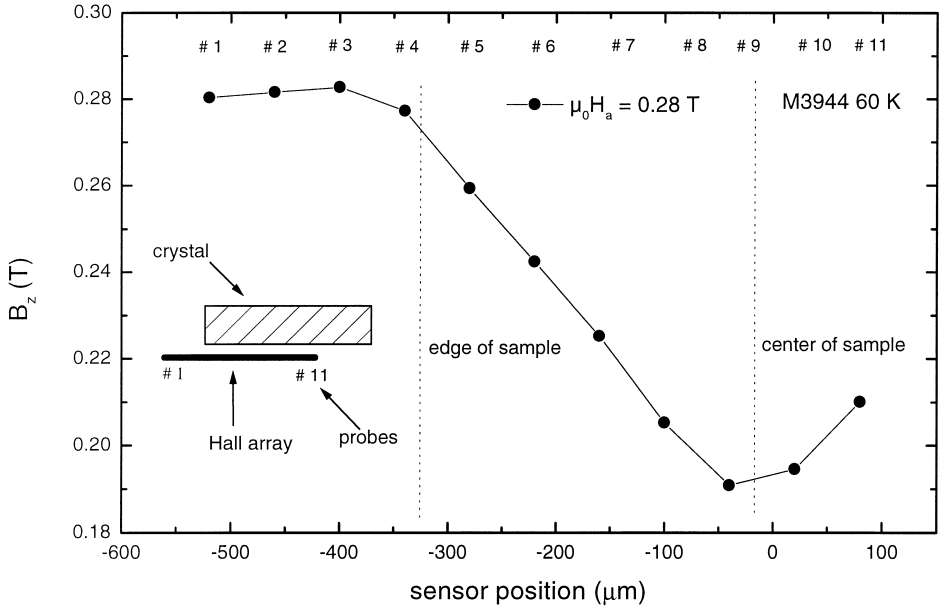

Fig. 1. Field profile within the sample measured by the local Hall probe technique.

is a very small displacement of the springs with respect to each other, which can be measured by applying an AC voltage between the plates of a capacitor and by detecting the capacitance with a lock-in amplifier via a capacitance bridge. The ratio between the torque and the change in capacitance is calibrated by applying a known torque with a calibration coil.

The spring constant of the phosphorus bronze springs is chosen so as to guarantee a linear response of the torquemeter over the whole range of signals of interest.

The shielding current density J_s is calculated by assuming that the currents are distributed according to the extended Bean model [8]. Beside field loops at different sweep rates (dynamical relaxation), conventional relaxation measurements were done, where the decay of the torque signal was monitored over a certain time interval (20 min). The normalized conventional relaxation rate R is defined as the normalized logarithmic time derivative of the magnetic moment $|\boldsymbol{m}|$ of the sample [11],

$$R \equiv -\frac{\mathrm{d}\ln|\boldsymbol{m}|}{\mathrm{d}\ln t}. \tag{3}$$

Together with Eq. (2), we obtain

$$\frac{\mathrm{d}\ln|\boldsymbol{m}|}{\mathrm{d}\ln t} = \frac{\mathrm{d}\ln(\tau/B\sin\alpha)}{\mathrm{d}\ln t} = \frac{\mathrm{d}\ln\tau}{\mathrm{d}\ln t} - \frac{\mathrm{d}\ln B}{\mathrm{d}\ln t} - \frac{\mathrm{d}\ln(\sin\alpha)}{\mathrm{d}\ln t}. \tag{4}$$

Since the applied field and the angle are kept constant ($\dot{B}=0$, $\dot{\alpha}=0$) during the measurement, only the first term is of importance. Thus, the relaxation rate can be obtained immediately from the measured data. The time t_0, which describes the moment, where the relaxation starts, is defined by the end of the field sweep. As we are interested in the relaxation for $t \geq 10$ min, the transition period between the field sweep and the constant field modes of the magnet [12] can be neglected.

2.4. Hall probe arrays

While we used in the present work MO-measurements only for gathering qualitative information about the way the magnetic flux penetrates the sample, the local Hall probe technique was employed for a quantitative assessment of the magnetic induction $\boldsymbol{B}$ profile. This method was invented many years ago

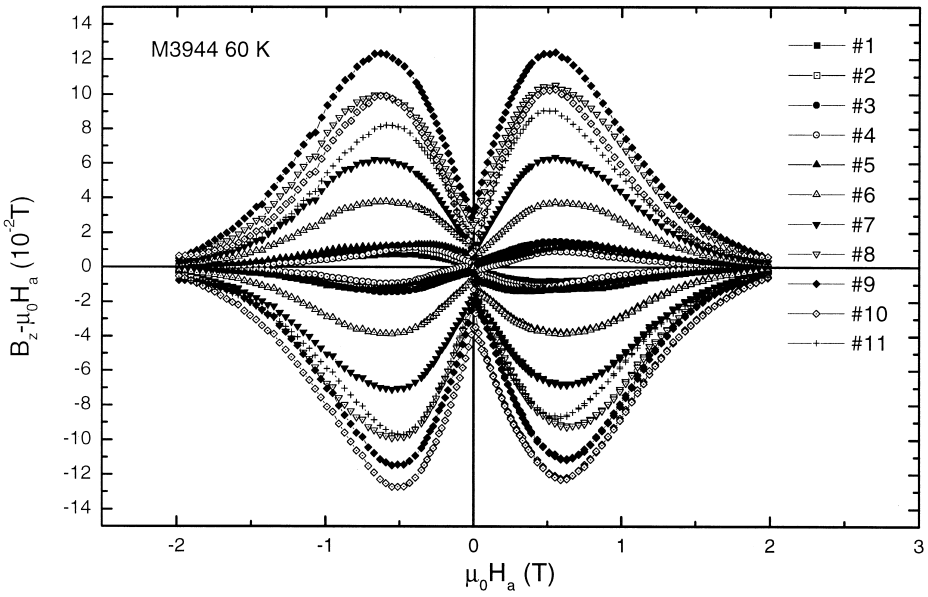

Fig. 2. Typical hysteresis loop obtained with Hall sensors at different locations on the sample surface.

[13,14], but improved recently by the development of arrays of Hall sensors based on a two dimensional electron gas (2DEG) by etching a mesa into the GaAs/AlGaAs heterostructure which defines the Hall configuration [15].

Measurements up to 1.5 T with field steps of the order of 0.05 T were done (the temperature stability was 0.01 K). The currents through the probes were typically between 0.1 and 0.2 mA. Thus, heating of the sample by the current is negligible. The Hall probe array [3] consists of 11 elements with an active area of 30 μm $\times$ 30 μm of each probe and a resolution of better than 10^{-5} T.

Theoretically, these sensors are characterized by a linear response to the magnetic field, a weak temperature dependence and a high sensitivity. This is valid only in a certain field range (e.g., $\leq$ 1.5 T at $\geq$ 60 K). In higher fields the linearity gets lost and results in a more difficult evaluation of the data. Due to this reason most published data are obtained in a temperature range near the critical temperature at fields $\leq$ 1 T. As the Hall constant is also a function of T, a calibration at each temperature has to be done—similar to torque measurements. Furthermore, each probe has to be treated separately, as there are always small differences between them resulting in a slightly different sensitivity. Mounted inside the cryostat on a temperature controlled sample holder with the external field parallel to the crystallographic c-axis, the probes detect the $\hat{z}$-component of the field perpendicular to the surface of the crystal (see also Fig. 1). Fig. 2 shows a typical result of magnetization curves.

The evaluation of the current density is done by fitting the profile of the local magnetic induction to the calculated B_z obtained from the Biot–Savart law, considering a slab geometry with a long thin superconducting strip of rectangular cross-section of width $2w$ ($-w \leq x \leq w$), thickness d ($-d/2 \leq z \leq d/2$) and length $L \gg w$. Furthermore, a constant current density flowing only in one direction at the location of the probes is assumed. The distance of the probes from the surface of the sample is about 3 μm. Thus, the Biot–Savart law implies for the $\hat{z}$-

[3] Produced at the Weizmann Institute.

component of the magnetic induction B:

$$B_z = \mu_0\left(H + \frac{J}{4\pi}\int_{-d/2}^{d/2} \times \ln\left[\frac{((x+w)^2+(z-z')^2)((x-w)^2+(z-z')^2)}{(x^2+(z-z')^2)^2}\right]\mathrm{d}z'\right) \quad (5)$$

For this reason, only the middle part of the sample is investigated by this method, which makes the assumption reasonably good [3,16].

These microscopic techniques, MO and Hall probe arrays, result in much more detailed information on the mixed state than global magnetization measurements do. For example, Zeldov et al. [17] were able to distinguish between a Bean like and a geometrical barrier controlled behavior and Giller et al. [18] demonstrated with Hall probe arrays the importance of geometrical barriers in $Nd_{1.85}Ce_{0.15}CuO_{4-\delta}$ single crystals. By a quantitative analysis of MO images, Wijngaarden et al. [19] showed the influence of twin planes on the flux movement and current flow.

3. Results and discussion

3.1. SQUID–torque

When comparing these two techniques, one has to take their different time scales into consideration. For the HF-SQUID the time table for taking one data point is as follows: After a field change and a waiting time of 10 min, the measuring cycle starts, which lasts for 5 min. Between each field step the temperature stability is checked. Up to 5.5 T the sweep rate of the magnet is 14.92 mT/s and 1.33 mT/s above. In contrast to the SQUID, the torquemeter enables continuous measurements at different sweep rates of the magnet (40, 30, 20, 10, 5 mT/s). A disadvantage of torque magnetometry is the necessity of applying the external field at an angle to the main crystallographic directions. However, according to Klein et al. [20], slight misalignments can be neglected for angles less than 10° in the region around $H \| c$.

A typical experimental result is presented in Fig. 3. The lowest solid line refers to the data obtained from SQUID measurements. Taking the time interval

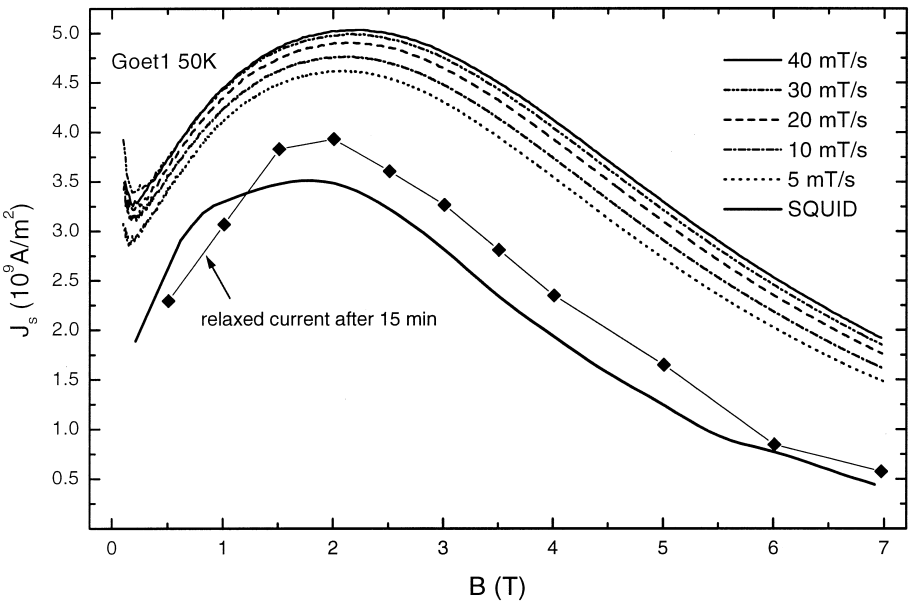

Fig. 3. Superconducting shielding current density J_s determined from torque and SQUID measurements at 50 K; the symbols (diamond shape) result from conventional relaxation measurements (40 mT/s) indicating the decrease of $J_s(t)$ after 15 min.

for stabilization into consideration, the decrease of the current $J_s(t)$ extracted from conventional relaxation measurements for a time interval of 15 min, results in the diamond symbols in Fig. 3. We can neglect the transition period between the field sweep and the constant field modes of the magnet. The same holds for the different sweep rates of the relaxation and the SQUID measurements. The remaining small difference is explained as follows. The torque is monitored continuously while changing the external field at a constant sweep rate. In contrast, SQUID experiments scan the magnetization point by point with extended waiting times in between. Thus, the history of the profile is different at each point.

3.2. SQUID–VSM

Nearly the same arguments hold for a comparison between SQUID and VSM. The vibrating sample magnetometer used for the measurements was a VSM3001 from Oxford Instruments. The set-up consists of a temperature and magnetic field control unit, the vibrator, a VTI, a low-loss cryostat, and a vertical magnet. All measurements were made with a sweep rate of 20 mT/s in fields up to 12 T applied parallel to the crystallographic *c*-axis. The sample was mounted onto a perspex sample holder, which was fixed onto a carbon rod. The carbon rod was mounted onto the vibrator. The sample was moved with an amplitude of 1.5 mm (peak to peak) at a frequency of 66 Hz. Similar to torque magnetometry the data are continuously measured during the experiments. Thus, the same arguments concerning the different time scale of the methods also hold in case of the vibrating sample magnetometer (Fig. 4).

3.3. SQUID–Hall probe array

So far, we compared only macroscopic methods, where the current density is derived based on the assumption that the flux profile behaves more or less according to the Bean model. Fig. 1 confirms such a Bean-profile inside the crystal. To evaluate the current density, this profile of the local magnetic induction B_z^i is fitted to the Biot–Savart law. We assume that $J_c(B) = \text{constant}$ (Bean) and that only B_z is relevant due to the slab geometry of the sample. The component B_x is not important anyway as long as a field of reasonable size is on, which is easily fulfilled for fields above the Bean penetration field. Despite these assumptions the agreement between the results

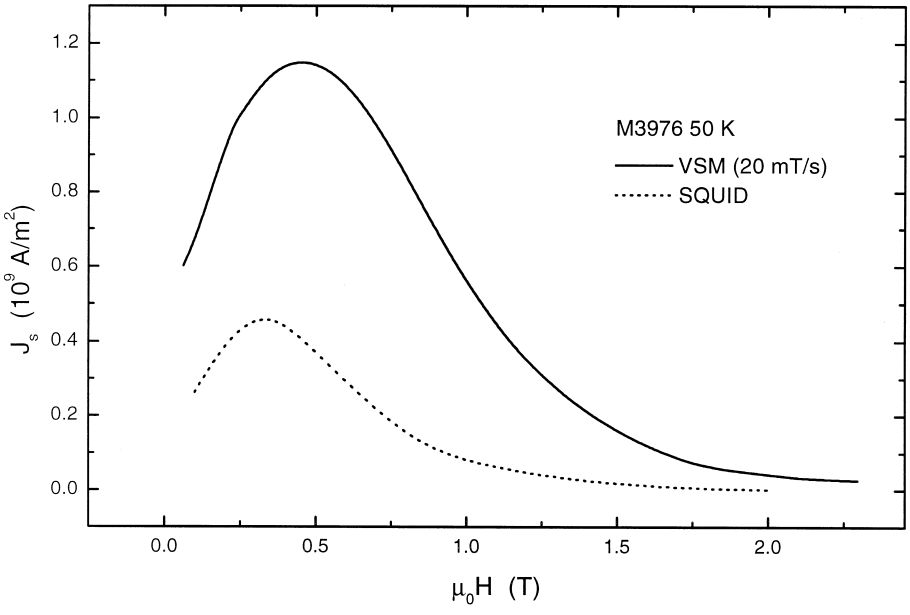

Fig. 4. Superconducting shielding current density J_s determined from VSM and SQUID measurements at 50 K.

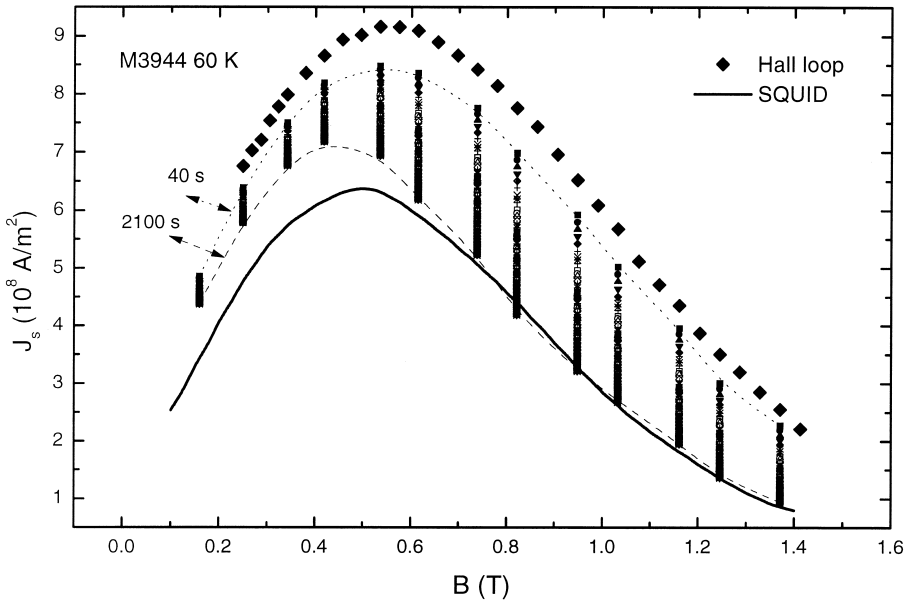

Fig. 5. Superconducting shielding current density J_s determined from local Hall probe and SQUID measurements at 60 K (M3944).

obtained with this new technique and those measured in the SQUIDs, is excellent as shown in Fig. 5. The time dependence of the maximum is clearly visible and shifts to lower fields with increasing time. This is in agreement with the results of torque magnetometry and VSM.

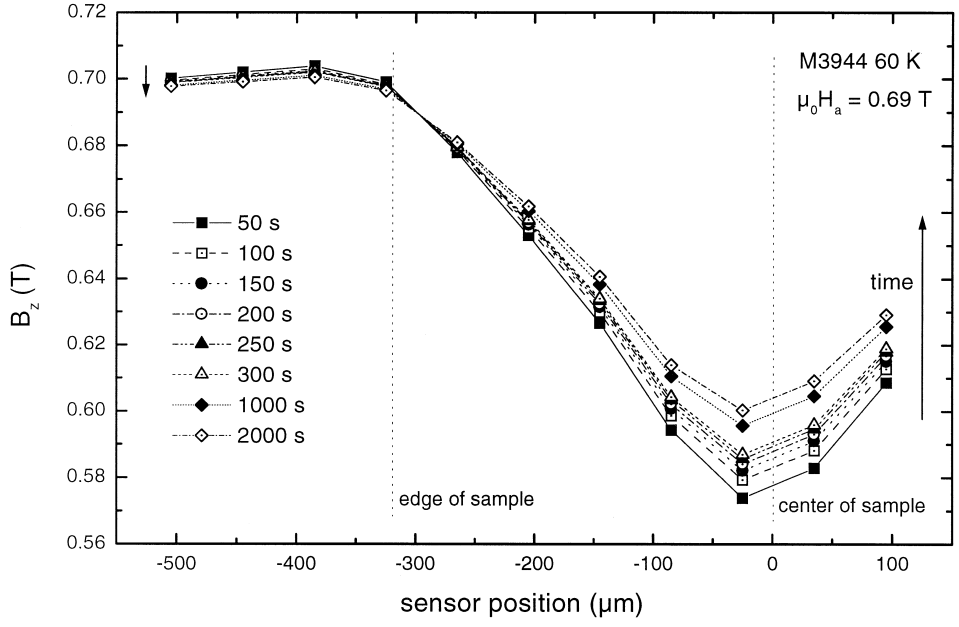

Fig. 6. Flattening of the induced Bean profile with increasing time.

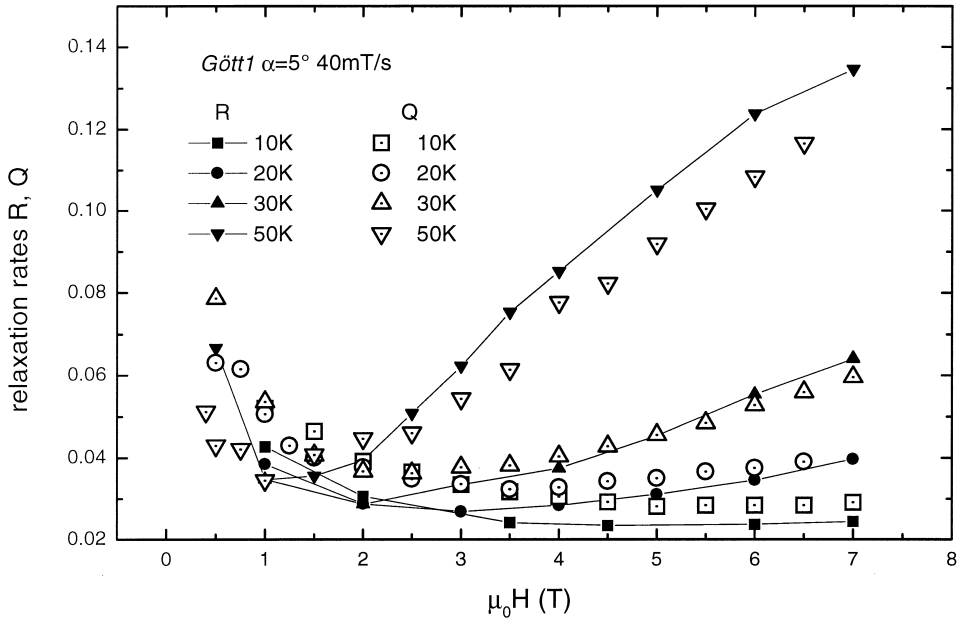

Fig. 7. Comparison between R and Q at several temperatures.

3.4. Relaxation

Thermal activation induces a finite probability for spontaneous depinning of vortices. For HTS this possibility of thermal depinning is enhanced due to the small coherence length ξ, the large magnetic penetration depth λ and the high anisotropy. Fig. 6 demonstrates the time evolution of the local induc-

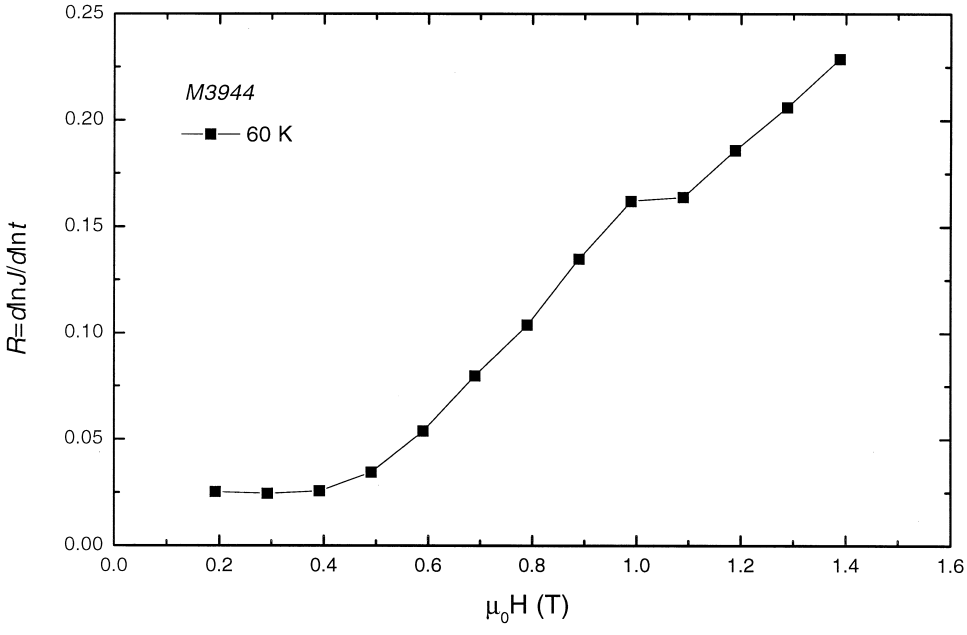

Fig. 8. Conventional relaxation rate R determined from the Hall array measurements.

tion inside and outside the sample. Therefore, two different types of measurements were made by torque magnetometry. Firstly, the conventional relaxation, $R = (-\mathrm{dln}\ J_s/\mathrm{dln}\ t)$, was monitored over a time period of 20 min. Secondly the dynamical relaxation [21,22], $Q \equiv (\mathrm{dln}\ J_s/\mathrm{dln}(\mathrm{d}B/\mathrm{d}t))$, was measured. According to Eq. (1), R can be immediately extracted from the time dependence of the measured signal. The field steps between two consecutive conventional relaxation measurements were twice as large as the Bean penetration field and the relaxation was monitored both on the increasing and the decreasing branch of the magnetization loop. Thus, the relaxation starts from a well defined (fully penetrated) state. Since the irreversible magnetization depends on the sweep rate $\mathrm{d}B/\mathrm{d}t$ of the external magnetic field, the dynamical relaxation rate, Q, was obtained from magnetization loops at various sweep rates. At low temperatures (below 10 K) both R and Q decrease with increasing field. This behavior changes completely with increasing temperature, leading to higher rates at higher magnetic fields already at 30 K.

A comparison between conventional and dynamical relaxation is shown in Fig. 7. We find excellent agreement between these two techniques at all investigated fields and temperatures. This agrees well with results obtained by van Dalen on $Bi_2Sr_2CaCu_2O_8$ crystals [23].

The strong increase of R at higher temperatures is also observable in the Hall probe measurements. Fig. 8 shows the results at 60 K, which were evaluated from the data depicted in Fig. 5. The higher values of R compared to those from torque magnetometry correspond to the faster response time of the Hall probe experiment.

4. Summary

We presented a comparison between the most common 'global' magnetization measurement methods, SQUID, torque and vibrating sample magnetometer, as well as between a global technique (SQUID) and a local one (Hall probe array). Taking the different time scales of the various types of measurements into account we obtain excellent agreement. Especially, the correlation between the SQUID and the Hall probe measurements, established by the present experiments, prove that the Hall probe array is not only an equivalent technique for investigating single crystalline samples, but even preferable, because more microscopic information on the local field distribution within the crystals becomes accessible.

To complete the analysis of the mixed state, relaxation measurements were performed with a torque magnetometer as well as with the Hall probe array. Dynamical and conventional relaxation rates agree very well with each other. At low temperatures, a decrease of the relaxation rates with increasing field is observed, while at higher temperatures increasing relaxation rates above a minimum are found.

Acknowledgements

This work was supported in part by the Austrian Ministry of Research and Transport under contract No. 185/3-IV/6/94 and by the HCM program of the European Union. One of us (M.W.) wishes to thank R. Griessen and Y. Yeshurun for their great hospitality during his stays at the Vrije Universiteit in Amsterdam and at Bar Ilan University, Israel. H.W.W and Y.Y. acknowledge support through an Austrian–Israeli Exchange Program administered by the Ministry of Science and Technology. Y.Y. acknowledges support from the Heinrich Hertz Minerva Center for High Temperature Superconductivity and the Israel Science Foundation. Work at Argonne National Laboratory was supported by the U.S. Department of Energy under contract No. W-31-109-ENG-38.

References

[1] C.P. Bean, Phys. Rev. Lett. 8 (1962) 250.
[2] C.P. Bean, Rev. Mod. Phys. 36 (1964) 31.
[3] Y. Abulafia, A. Shaulov, Y. Wolfus, R. Prozorov, L. Burlachkov, Y. Yeshurun, D. Majer, E. Zeldov, V. Vinokur, Phys. Rev. B 75 (1995) 2404.
[4] R.J. Wijngaarden, H.J.W. Spoelder, R. Surdeanu, R. Griessen, Phys. Rev. B 54 (1996) 6742.
[5] J. Clark, Superconducting Quantum Interference Devices for Low Frequency Measurements, in: B.B. Schwartz, S. Foner, Superconductor Applications: SQUIDs and Machines, Plenum, New York, 1977.

[6] VTS-Susceptometer 800 Series, Manual, S.H.E.
[7] H.P. Wiesinger, PhD Thesis, TU-Wien, 1991.
[8] H.P. Wiesinger, F.M. Sauerzopf, H.W. Weber, Physica C 203 (1992) 121.
[9] R. Griessen, M.J.G. Lee, D.J. Stanley, Phys. Rev. B 16 (1977) 4385.
[10] R. Griessen, Cryogenics 13 (1973) 375.
[11] Y. Yeshurun, A.P. Malozemoff, A. Shaulov, Rev. Mod. Phys. 68 (1996) 3.
[12] H.G. Schnack, PhD Thesis, VU Amsterdam (1995).
[13] H.W. Weber, G.P. Westphal, I. Adaktylos, Cryogenics 16 (1976) 39.
[14] I. Adaktylos, E. Schachinger, H.W. Weber, J. Low Temp. Phys. 26 (1977) 533.
[15] D. Majer, E. Zeldov, H. Shtrikman, M. Konczykowski, Coherence in high-T_c superconductors, in: A. Revcolevschi, G. Deutscher, World Scientific Publishing, Singapore, p. 271 (1995).
[16] Y. Abulafia, A. Shaulov, Y. Wolfus, R. Prozorov, L. Burlachkov, Y. Yeshurun, D. Majer, E. Zeldov, V.M. Vinokur, Coherence in high-T_c superconductors, in: A. Revcolevschi, G. Deutscher, World Scientific Publishing, Singapore, p. 297 (1995).
[17] E. Zeldov, A.I. Larkin, V.B. Geshkenbein, M. Konczykowski, D. Majer, B. Khaykovich, V.M. Vinokur, H. Shtrikman, Phys. Rev. Lett. 73 (1994) 1428.
[18] D. Giller, A. Shaulov, R. Prozorov, Y. Abulafia, Y. Wolfus, L. Burlachkov, Y. Yeshurun, E. Zeldov, V.M. Vinokur, J.L. Peng, R.L. Greene, Phys. Rev. Lett. 79 (1997) 2542.
[19] R.J. Wijngaarden, R. Griessen, J. Fendrich, W.K. Kwok, Phys. Rev. B 55 (1997) 3268.
[20] L. Klein, E.R. Yacoby, Y. Yeshurun, A. Erb, G. Müller-Vogt, V. Breit, H. Wühl, Phys. Rev. B 49 (1994) 4403.
[21] L. Pust, J. Kadlecova, M. Jirsa, S. Durcok, J. Low Temp. Phys. 78 (1990) 179.
[22] M. Jirsa, L. Pust, H.G. Schnack, R. Griessen, Physica C 207 (1995) 85.
[23] A.J.J. van Dalen, PhD Thesis, VU Amsterdam (1995).